Boletim da Sociedade Astronômica Brasileira, **33**, no. 1, 113-117

Low-ionization structures in planetary nebulae: statistically strengthening the molecular counterpart argument

M. Belén Mari[1], Denise R. Gonçalves[1], & Stavros Akras[2]

[1] Observatório do Valongo, Universidade Federal do Rio de Janeiro, Ladeira Pedro Antonio 43, Rio de Janeiro 20080-090, Brazil
e-mail: mbmari@astro.ufrj.br
[2] Institute for Astronomy, Astrophysics, Space Applications and Remote Sensing, National Observatory of Athens, Penteli GR 15236, Greece

Abstract. Here we present the optical, intermediate-resolution spectroscopic analysis of 2 from a sample of 6 planetary nebulae (PNe), in a spatially-resolved fashion, where low-ionization structures (LISs) are contrasted with their host PN main-structures. Subsequently, by using these new data together with similar studies published previously, we perform a robust statistical analysis of the most complete sample of LISs in PNe gathered together so far. In terms of electron densities, electron temperature and chemical abundances, our results show no important discrepancy with the conclusions obtained from smaller samples, and clearly reinforce the idea that only the molecular counterpart of LISs could effectively help to solve the open questions related with the origin of these structures.

Resumo. Apresentamos aqui a análise de espectros ópticos de resolução intermediária para 2 de uma amostra de 6 nebulosas planetárias (PNe), onde as várias componentes são resolvidas, de forma que as estruturas de baixa ionização (LISs) são contrastadas com as estruturas principais das PNe hospedeiras. Posteriormente, utilizando estes novos dados juntamente com estudos similares publicados anteriormente, realizamos uma análise estatística robusta da, até o momento, mais completa amostra de LISs em PNe. Em termos de densidade e temperatura eletrônicas e abundâncias químicas, nossos resultados não mostram nenhuma discrepância importante com as conclusões obtidas com amostras menores, e reforçam claramente a idéia de que somente a confirmação da contrapartida molecular das LISs poderia efetivamente ajudar a resolver as questões abertas sobre a origem dessas estruturas.

Keywords. ISM: abundances – ISM: jets and outflows – planetary nebulae: individual: NGC 3918, NGC 6543.

1. Introduction

Planetary nebulae (PNe) are formed after the asymptotic giant branch (AGB) evolutionary stage of low- and intermediate-mass stars (0.8-8$M_{\odot}$). In that phase of the stellar evolution, the outer layers of the stellar atmosphere are ejected due to thermal pulses enriching the interstellar medium. The central stars of PNe are the nucleus of the progenitor stars, which become exposed after the ejection of the outer material, and are roughly characterized by $T_{eff} \geq 50000$ K and log(L) between 3 and 4 (for a recent compilation, see Weidmann et al. 2020). The ejected material is subsequently ionized by the photon flux from these stars.

Any (morphological) classification of PNe relies on the (shape of) their large-scale nebular components such as rims, attached shells and haloes, mainly identified by bright Balmer series lines and collisional excitated lines from [O III]. They are divided into five main classes: point-symmetric, elliptical (that includes round), bipolar, multipolar and irregular (Manchado et al. 1996).

In addition, it is known that PNe possess a number of small-scale structures that, at variance with their large-scale structures, are prominent in optical low-ionization lines such as [N II], [S II], [O I] and [O II] (Corradi et al. 1996; Balick et al. 1998; Gonçalves et al. 2001; Akras & Gonçalves 2016). It is important to note that the spatial resolution is crucial for studying these structures, therefore we can not perform such an analysis for extragalactic PNe, while by studying these kind of object in our Galaxy we can infer the behavior/properties in the extragalactic ones. One of the ways to find these structures is by using narrow-band imaging of PNe in low- and high-ionization lines as was performed by Corradi et al. (1996), in which the ratio of two narrow-band images, Hα+[N II] and [O III], highlights these structures.

Diverse works have been carried out to study the low-ionization structures (LISs) in an attempt to understand their formation processes using the long-slit spectroscopy (e.g. Balick et al. 1993, 1994; Hajian et al. 1997; Gonçalves et al. 2003, 2004, 2009; Akras & Gonçalves 2016, among others). The general conclusions drawn so far are as follows: (i) the electron temperatures (T_e) of LISs and of the main components of the host PNe are similar, (ii) electron densities (N_e) in LISs are usually lower (or at most equal) than in the main structures, and (iii) there are no large variations in chemical abundances between LISs and other nebular components. Contrarily, theoretical predictions suggest that LISs should be denser than the inner regions, by at least a factor of ~10. Therefore to reconcile models and observations Gonçalves et al. (2009) suggested that an important fraction of the LISs – 90 per cent – should be atomic and molecular gas (see, for instance, Akras et al. 2017).

In order to provide further insight for the origin of the LISs, we performed intermediate-resolution spectroscopic analysis of six PNe, in a spatially resoved fashion, and here we present some of the results, for 2 of them (NGC 3918 and NGC 6543).

2. Observations and nebular diagnostics

NGC 6543 was observed (in August of 2001) with the Intermediate Dispersion Spectrograph (IDS) at the 2.5m Isaac Newton Telescope (INT) by using a configuration that gives 0.70 arcsec pixel^{-1} and 3.3 Å pixel^{-1} and covers from 3650 to 7000 Å, with a slit width (length) of 1.5 arcsec (4 arcmin). For the case of NGC 3918 the 1.54m Danish telescope was used,

with the DFOSC camera, which resulted in a spatial scale of 0.40 arcsec pixel^{-1}, a wavelength range of 3600-8000 Å and a spectral resolution of 2.2 Å pixel^{-1}; the observations were performed on April 1997, and the slit width and length were 1.0 arcsec and >13.7 arcmin, respectively.

Taking into account the different positions in which the LISs are found in these nebulae, spectra were obtained using more than one position angle (PA), as well as different exposure times. The LONGSLIT package of IRAF was used for the standard procedure of reduction and analysis of the data.

The Nebular Empirical Analysis Tool (NEAT, Wesson et al. 2012) was employed to identify the lines, estimate the extinction coefficient (c_β) –using the flux-weighted ratios of Hα, Hγ and Hδ to Hβ– and correct the line fluxes by adopting $R_V = A_V/E(B-V) = 3.1$ as the reddening law (Howart 1983). NEAT also was applied to derive the electron temperatures (T_e) and densities (N_e) and the ionic and as well as total abundances (X/H).

3. Results

3.1. From our own sample

Figure 1 presents two PNe of the whole sample observed (Mari et al. 2022, in prep.). Part of the results of our spectroscopic analysis for different morphological structures such as LISs, shells, rims and a region we defined as Neb (generally of high-ionization that integrates the emission of different structures of the nebula, along a given PA) are summarized here.

Tables 1 and 2 display the analyses of NGC 3918 and NGC 6543, two representative examples of our sample, in which it is shown the spatial variation of T_e, N_e and X/H across nebular components.

3.1.1. NGC 3918

The electron temperature using both [N II] and [O III] diagnostic lines is almost constant through components and slit positions, and it is also consistent with the values in the literature (Clegg et al. 1987; Richer et al. 1991; Kwitter et al. 2003; Henry et al. 2004; García-Rojas et al. 2015). For the case of [O III], there is one of the LIS (B") whose temperature is higher than in the rest of the structures, although the uncertainty of this quantity is as well much higher.

The electron density using [S II] diagnostic lines is almost constant through the main components, having an average value of 5225±190 cm^{-3}, which is consistent with the previously published estimations (Stanghellini & Kaler 1989; Phillips 1998; García-Rojas et al. 2015). Regarding the LISs, it can be noted that their electron densities are lower in comparison with the main structures, by a factor which varies from ∼2.6 to ∼3.9.

The total abundance of He has no contrast through the nebular components, with an average value of 0.104±0.003, in good agreement with the published values (Perinotto 1991; Kwitter et al. 2003; Henry et al. 2004, 2018). For oxygen and neon abundances, there is no much variation among nebular components, except for the LIS B", for which we find, respectively, an abundance of approximately half and a factor of ∼5.7 lower than for the other structures. Excluding this LIS, the average value of O/H is (4.0±0.1)×10^{-4} – lower than those published by Perinotto (1991); Kwitter et al. (2003); Henry et al. (2004), but in agreement with Henry et al. (2018). For the case of Ar/H, our values are lower than those reported by Kwitter et al. (2003); Henry et al. (2004), whereas the average Cl/H and S/H are consistent with those published by Kwitter et al. (2003).

3.1.2. NGC 6543

This nebula, also known as Cat's Eye, shows no variation of the electron temperature among the nebular components. The face values of its T_e, being in good agreement with the literature: in the case of [N II] with Wesson & Liu (2004); Williams et al. (2008) and in the case of [O III] with Phillips (1998); Robertson-Tessi & Garnett (2005).

Regarding the N_e [S II], we can observe a subtle variation among the nebular components, mainly for the LISs (J and J') whose values are much lower than those of the shell and Neb by a factor ∼5.3 for J and ∼5.5 for J'. The comparison with the literature (Wesson & Liu 2004; Williams et al. 2008) shows that the results obtained in this work are consistent with the previously reported.

As for the total abundances, Table 2 shows a slight variation of He/H across the components, nevertheless taking the errors into account, the values are in good agreement with the literature (Kaler 1970; Perinotto et al. 1999; Hyung et al. 2000; Perinotto et al. 2004). For the oxygen abundances, there is no much variation among the components, except for both LISs located along PA=5°, for which O/H are lower than in the main components, and the latter abundances are in good agreement with the reported ones (Perinotto et al. 1999; Hyung et al. 2000; Perinotto et al. 2004). On the other hand, for N/H we can observe a small variation through the slits and components, having the highest values for A and D rims and also for the LIS named J'. This variation was previously reported by Balick et al. (1994). The Ne/H also shows variations across the components, though the average values are in good agreement with the literature (Perinotto et al. 1999; Hyung et al. 2000; Perinotto et al. 2004). The Ar abundances present subtle variations, but note that Ar/H were invaluable for the LISs. For Neb, the Ar abundance is consistent with Kaler (1970); Perinotto et al. (2004), considering the errors, but lower than those reported by Perinotto et al. (1999); Hyung et al. (2000).

3.2. From the statistically robust sample

In order to characterize LISs and the main structures of the PNe, we gathered together all the available data from the literature (Balick et al. 1994; Hajian et al. 1997; Gonçalves et al. 2003, 2004, 2009; Danehkar et al. 2016; Akras & Gonçalves 2016; Ali & Dopita 2017; Monreal-Ibero & Walsh 2020; Miranda et al. 2021) and combined them with the new data of our sample of 6 PNe (two of them presented in Figure 1), so increasing the total sample to study (Mari et al. 2022, in prep.).

To interpret the collective properties of the PNe with LISs, using the total sample, we took advantage of the statistical representation given by violinplots, which combine boxplots and kernel density distributions in one diagram (Hintze & Nelson 1998). These plots show the median, quartiles and interquartile range (IQR), as well as any possible asymmetry in their distribution. Note that violinplots can provide information about the shape of the distribution such as their peaks and their positions, or even unveil the presence of clustering in the data (e.g. a bimodal distribution). Inside these violinplot we have boxplots, which are useful to compare distributions for different groups. For this more detailed comparison it is necessary, according to Chambers et al. (2017), to estimate the notches on the sides of their medians to analyze the relative location between samples. These notches can be used to demonstrate the 95 percent of confidence interval (CI) for the median. When these notches do not overlap, the medians of the distributions can be judged to differ significantly (Krzywinski & Altman 2014), but a possible

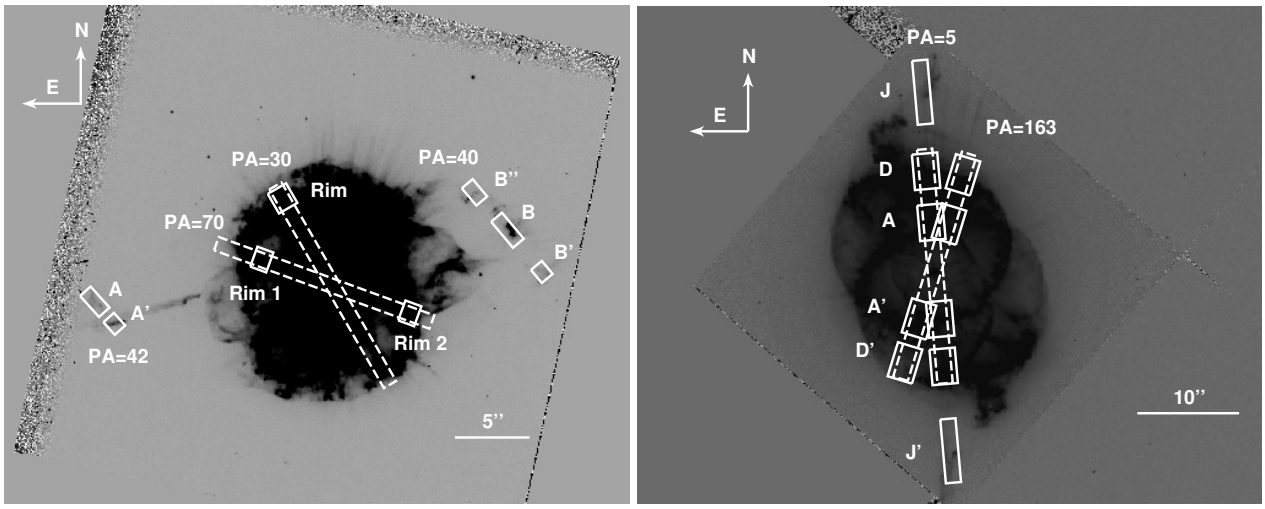

Figure 1. [N II] images for two PNe of our sample (Mari et. al. 2022, in prep.). The images are from the HST archive. Nebular components selected for the spectroscopic analysis are highlighted. *Left panel:* NGC 3918 with its LISs (A, A', B, B' and B"), rims/shells (Rim, Rim1 and Rim 2) and Neb (dashed lines). *Right panel:* NGC 6543 with its LISs (J and J'), rims/shells (A, A', D, D') and Neb (dashed lines). The sizes of the fields are 43×34 and 61×48 arcsec^2, for NGC 3918 and NGC 6543 respectively.

Table 1. Physics and chemical parameters of NGC 3918: T_e(K), N_e(cm^{-3}) and total abundances.

NGC 3918		Te[NII]	Te[OIII]	Ne[SII]	He/H(×10^2)	O/H(×10^4)
PA=30	Neb	11100±530	12700±170	5070±220	10.4±0.1	3.8±0.1
	Rim	10700±620	12100±220	5720±250	9.3±0.2	3.8±0.1
PA=70	Rim1	11300±520	12000±250	5450±220	9.9±0.2	4.1±0.1
	Neb	11200±820	12700±210	5380±310	10.3±0.2	3.9±0.1
	Rim2	11000±980	12700±240	5710±290	11.0±0.2	4.0±0.1
PA=40	B'	9430±3675	12500±1600	1620±324	9.4±1.1	4.2±0.6
	B	11300±2675	12600±1550	2030±360	10.6±1.0	4.0±0.7
	B"	10000±4660	16300±3800	1920±397	10.3±1.7	1.7±0.5
PA=42	A'	10900±1520	12400±890	1340±127	11.3±1.3	4.1±0.4
	A	11100±1380	12700±600	1860±111	11.3±0.7	4.2±0.3
		N/H(×10^5)	Cl/H(×10^8)	Ne/H(×10^5)	S/H(×10^6)	Ar/H(×10^6)
PA=30	Neb	13.2±0.9	10.5±1.1	7.4±0.2	3.9±0.5	1.43±0.04
	Rim	12.4±1.0	10.7±1.0	7.2±0.2	4.1±0.5	0.77±0.02
PA=70	Rim1	15.3±1.1	11.6±1.1	9.0±0.3	5.6±0.7	0.91±0.04
	Neb	12.0±1.1	11.0±1.4	7.6±0.2	4.2±1.0	1.48±0.05
	Rim2	11.6±1.1	13.7±1.1	7.4±0.2	4.1±1.0	1.34±0.04
PA=40	B'	18.3±3.8	-	8.8±1.6	2.3±1.2	0.68±0.23
	B	20.8±3.9	-	8.0±1.3	2.6±1.1	0.84±0.24
	B"	16.4±3.9	-	1.4±0.7	3.7±2.2	0.39±0.25
PA=42	A'	15.7±1.6	-	8.6±0.9	4.7±1.2	0.53±0.09
	A	17.0±1.3	11.6±2.2	8.4±0.6	3.7±0.9	0.67±0.06

overlap does not necessarily rule out the possibility that the two samples are different.

When we performed the distributions of electron temperatures and densities for the nebular components studied in this work –Neb, rims/shells and LISs–, taking into account the median and IQR, it was easily perceptible that Neb and rim/shells were very similar, while the low-ionization structures formed an apparently different group. This fact is shown in Figure 2, where the distributions of these quantities are presented in split violinplots, which contrast two groups, rims/shells with LISs. The comparison is detailed in Table 3, by showing the median, notches, sample's number and outliers, of the two groups. We can see that for T_e [N II], the distributions are very similar with close median values and upper/lower notches. The case of T_e [O III] is different, the notches do not overlap and we can observe that the shape of the distribution for rims/shells is slightly bimodal. From the analysis of log(Ne[S II]) of the different samples, it is straightforward noticing that effectively, the notches do not overlap! Moreover, this behaviour could be anticipated considering the results in the literature (and in the current work), where LISs tend to have lower electron density than the main, high-ionization nebular components.

4. Remarkable conclusions

As previously mentioned, Gonçalves et al. (2009) contrasted a more limited sample of pairs of LISs in PNe with models, pointed out the discrepant densities observed (electron densities) and proposed that an important fraction of the LISs' matter should be atomic and molecular gas. Collecting information about the physical properties of the host PNe and LISs available in the literature, we conclude that the low electron density of these structures is a general property for the great majority of the LISs in PNe. Therefore, the hypothesis that the "missing mass" is in neutral state is strongly re-enforced by the present work. Indeed the most abundant molecules in Universe are H_2

Table 2. Physics and chemical parameters of NGC 6543: T_e(K), N_e(cm^{-3}) and total abundances.

NGC 6543		Te[NII]	Te[OIII]	Ne[SII]	He/H($\times10^2$)	O/H($\times10^4$)
	J	8340±3731	12100±7487	951±242	11.5±2.8	2.9±1.2
	D	9820±801	8300±796	4280±161	9.8±0.2	4.7±0.5
	A	10200±1251	8140±390	5390±241	11.8±0.1	5.3±0.3
PA=5	Neb	10200±1459	8310±724	5740±274	11.7±0.2	5.2±0.6
	A'	10600±1378	8360±368	5240±286	11.9±0.1	4.9±0.2
	D'	9930±397	8320±365	4660±97	12.3±0.2	5.5±0.3
	J'	11600±10908	10000±7167	926±211	12.4±2.4	3.2±1.4
	D	9460±544	8010±401	4310±142	11.7±0.2	5.8±0.3
	A	11000±1695	8180±409	5580±221	10.9±0.1	4.8±0.2
PA=163	Neb	9350±3189	8020±802	5870±366	12.1±0.2	5.8±0.7
	A'	9680±1054	8020±422	5620±210	11.2±0.1	5.5±0.2
	D'	10100±2024	7820±1235	4700±437	12.2±0.2	6.4±1.2
		N/H($\times10^5$)	Cl/H($\times10^8$)	Ne/H($\times10^5$)	S/H($\times10^6$)	Ar/H($\times10^7$)
	J	28.0±11.6	-	16.3±7.5	8.2±5.2	-
	D	58.3±8.8	29.1±4.9	22.3±2.2	10.9±2.2	2.7±0.8
	A	41.3±10.3	16.0±1.7	18.2±1.1	19.4±5.9	6.4±0.7
PA=5	Neb	17.5±2.7	17.7±5.8	14.3±1.9	14.1±5.2	5.7±1.2
	A'	30.2±4.9	14.9±1.3	14.3±0.7	16.3±5.0	6.7±0.5
	D'	29.1±2.3	32.5±7.6	25.5±1.6	23.5±2.9	2.0±0.5
	J'	54.8±28.0	-	16.4±8.3	5.8±4.7	-
	D	34.6±2.7	32.0±4.8	22.6±1.2	21.5±2.3	3.2±0.5
	A	15.6±2.5	12.4±1.0	13.9±0.8	17.3±5.8	6.4±0.4
PA=163	Neb	23.7±7.4	17.7±5.3	14.6±1.8	16.4±7.0	7.2±1.4
	A'	33.4±3.9	15.3±1.7	15.2±0.8	18.2±4.1	5.0±0.4
	D'	19.7±5.8	25.0±12.9	20.7±4.6	17.6±6.1	3.3±1.3

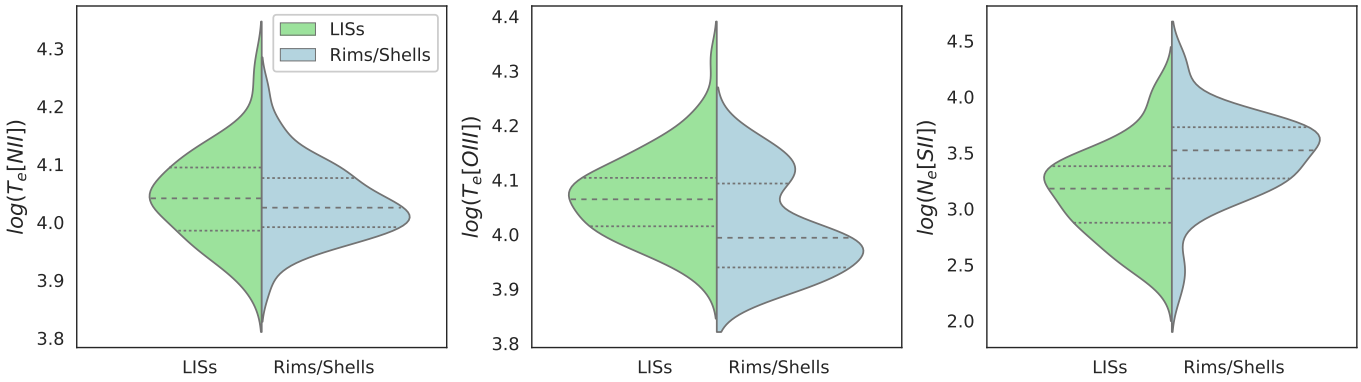

Figure 2. Comparison between nebular components, LISs and Rims/Shells, using split violinplots with the median (q2), 25th and 75th quartiles (q1 and q3) shown by dashed and dotted lines, respectively. The *notches* are not plotted because they are imperceptible at these scales (see Table 3).

Table 3. Properties of the two groups under analysis: Rims/Shells and LISs. The notches correspond to the approximated 95 per cent CIs. The last two rows show the number of outliers and sample size, respectively.

	log(T_e[N II])		log(T_e[O III])		log(N_e[S II])	
	Rims/Shells	LISs	Rims/Shells	LISs	Rims/Shells	LISs
Median	4.0253	4.0414	3.9921	4.0645	3.4909	3.1798
Lower notch	4.0067	4.0173	3.9594	4.0466	3.3943	3.0844
Upper notch	4.0439	4.0655	4.0248	4.0823	3.5874	3.2753
#Outliers	1	1	0	1	4	0
#Sample	51	56	59	61	60	69

and CO, and, so far, no CO observations have been carried out toward any PN with pairs of LIS. Nevertheless, as far as H_2 is concerned, it has been detected toward LISs of only a few PNe (Matsuura et al. 2009; Fang et al. 2015, 2018; Akras et al. 2017, 2020). Although still very limited, the works just quoted increased the number of LISs with H_2, further supporting the scenario that LISs are dense microstructures embedded in PNe, partially consisting of molecular gas, as suggested by the state of the art models (Balick et al. 2020). Therefore, a systematic H_2 and CO imaging and spectroscopic survey of PNe with LISs is required in order to understand how the molecular gas was formed or how it survived from the intense UV radiation and what is its dominant excitation mechanism.

Acknowledgements. This research is support by PhD grant from CAPES –the Brazilian Federal Agency for Support and Evaluation of Graduate Education within the Education Ministry of Brazil. DRG thanks the CNPq grants 428330/2018-5 and 313016/2020-8, and SA acknowledges the support under the grant 5077 by IAASARS/NOA.

References

Ali A., Dopita M. A., 2017, Publ. Astron. Soc. Australia, 34, e036
Akras S., Gonçalves D. R., 2016, MNRAS, 455, 930
Akras S., et al., 2017, MNRAS, 465, 1289
Akras S., et al., 2020, MNRAS, 493, 3800
Balick B., et al., 1993, ApJ, 411, 778
Balick B., et al., 1994, ApJ, 424, 800
Balick B., et al., 1998, AJ, 116, 360
Balick B., et al., 2020, ApJ, 889, 13B
Chambers J. M., et al., 2017, Graphical Methods for Data Analysis. 1st Edition, doi:10.1201/9781351072304
Clegg R. E. S., et al., 1987, ApJ, 314, 551
Corradi R. L. M., et al., 1996, A&A, 313, 913
Corradi R. L. M., et al., 2003, MNRAS, 340, 417
Danehkar A., et al., 2016, AJ, 151, 38
Fang X., et al., 2015, MNRAS, 452, 2445
Fang X., et al., 2018, ApJ, 859, 92F
García-Rojas J., et al., 2015, MNRAS, 452, 2606
Gonçalves D. R., et al., 2001, ApJ, 547, 302
Gonçalves D. R., et al., 2003, ApJ, 597, 975
Gonçalves D. R., et al., 2004, MNRAS, 355, 37
Gonçalves D. R., et al., 2009, MNRAS, 398, 2166
Hajian A. R., et al., 1997, ApJ, 487, 30
Henry R. B. C., et al., 2004, AJ, 127, 2284
Henry R. B. C., et al., 2018, MNRAS, 473, 241
Hintze J. L., Nelson R. D., 1998, The American Statistician, 52, 181
Howart I. D., 1983, MNRAS, 203, 301
Hyung S., et al., 2000, MNRAS, 318, 77
Kaler J. B., 1970, ApJ, 160, 887
Kingsburgh R. L., Barlow M. J., 1994, MNRAS, 271, 257
Kwitter K. B., et al., 2003, PASP, 115, 80
Magrini L., et al., 2012, IAU Symposium, 283, 251M
Manchado A., et al., 1996, The IAC morphological catalog of northern Galactic planetary nebulae.
Matsuura M., et al., 2009, ApJ, 700, 1067
Miranda L. F., et al., 2021, arXiv e-prints, p. arXiv:2105.05186
Monreal-Ibero A., Walsh J. R., 2020, A&A, 634, A47
Perinotto M., 1991, ApJS, 76, 687
Perinotto M., et al., 1999, A&A, 347, 967
Perinotto M., et al., 2004, MNRAS, 349, 793
Phillips J. P., 1998, A&A, 340, 527
Richer M. G., et al., 1991, ApJ, 377, 210
Robertson-Tessi M., Garnett D. R., 2005, ApJS, 157, 371
Stanghellini L. & Kaler J. B., 1989, ApJ, 343, 811
Weidmann W., et al., 2020, A&A, 640, 10W
Wesson R., Liu X. W., 2004, MNRAS, 351, 1026
Wesson R., et al., 2012, MNRAS, 422, 3516
Williams R., Jenkins E. B., Baldwin J. A., Zhang Y., Sharpee B., Pellegrini E., Phillips M., 2008, ApJ, 677, 1100